Science of the Total Environment 825 (2022) 153903

Contents lists available at ScienceDirect

Science of the Total Environment

journal homepage: www.elsevier.com/locate/scitotenv

Automatic quantification and classification of microplastics in scanning electron micrographs via deep learning

Bin Shi [a,*], Medhavi Patel [b], Dian Yu [a], Jihui Yan [a], Zhengyu Li [c], David Petriw [a], Thomas Pruyn [a], Kelsey Smyth [d], Elodie Passeport [b,d], R.J. Dwayne Miller [e], Jane Y. Howe [a,b]

[a] Department of Materials Science and Engineering, University of Toronto, ON M5S 3H5, Canada
[b] Department of Chemical Engineering and Applied Chemistry, University of Toronto, ON M5S 3E5, Canada
[c] Department of Mathematical and Computational Sciences, University of Toronto Mississauga, ON L5L 1C6, Canada
[d] Department of Civil and Mineral Engineering, University of Toronto, ON M5S 1A4, Canada
[e] Departments of Chemistry and Physics, University of Toronto, ON M5S 3H6, Canada

HIGHLIGHTS

- Image acquisition using variable-pressure scanning electron microscopes
- First open-source dataset of microplastics micrographs and segmentations
- High-performance segmentation and shape classification based on deep learning

GRAPHICAL ABSTRACT

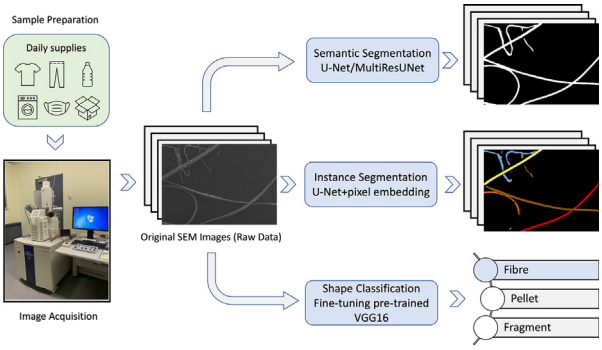

ARTICLE INFO

Article history:
Received 16 November 2021
Received in revised form 21 January 2022
Accepted 11 February 2022
Available online 19 February 2022

Editor: Kevin V. Thomas

Keywords:
Microplastics
Scanning electron microscopy
Image segmentation
Shape classification
Deep learning

ABSTRACT

Microplastics quantification and classification are demanding jobs to monitor microplastic pollution and evaluate the potential health risks. In this paper, microplastics from daily supplies in diverse chemical compositions and shapes are imaged by scanning electron microscopy. It offers a greater depth and finer details of microplastics at a wider range of magnification than visible light microscopy or a digital camera, and permits further chemical composition analysis. However, it is labour-intensive to manually extract microplastics from micrographs, especially for small particles and thin fibres. A deep learning approach facilitates microplastics quantification and classification with a manually annotated dataset including 237 micrographs of microplastic particles (fragments or beads) in the range of 50 μm–1 mm and fibres with diameters around 10 μm. For microplastics quantification, two deep learning models (U-Net and MultiResUNet) were implemented for semantic segmentation. Both significantly outmatched conventional computer vision techniques and achieved a high average Jaccard index over 0.75. Especially, U-Net was combined with object-aware pixel embedding to perform instance segmentation on densely packed and tangled fibres for further quantification. For shape classification, a fine-tuned VGG16 neural network classifies microplastics based on their shapes with high accuracy of 98.33%. With trained models, it takes only seconds to segment and classify a new micrograph in high accuracy, which is remarkably cheaper and faster than manual labour. The growing datasets may benefit the identification and quantification of microplastics in environmental samples in future work.

* Corresponding author.
E-mail address: binmse.shi@mail.utoronto.ca (B. Shi).

http://dx.doi.org/10.1016/j.scitotenv.2022.153903

1. Introduction

Plastic debris has entered the water body in recent years, which arouses general public concerns. Large-size plastics are easier to be discovered and filtered. In contrast, microplastics (MP), either primary plastic fragments or secondary plastics degraded from larger pieces, are less than 5 mm in size and some are invisible to human eyes. Microplastics have been reported to be ubiquitous in surface, subsurface and the deep sea (Woodall et al., 2014) of 5 major oceans (Desforges et al., 2014; Lusher et al., 2014; Isobe et al., 2014; Isobe et al., 2017; Lusher et al., 2015; do Sul and Costa, 2014), freshwater (Eerkes-Medrano et al., 2015; Wagner et al., 2014; Smyth et al., 2021; Werbowski et al., 2021), and lakes (Free et al., 2014). Microplastics digested will be detrimental to various living organisms and human beings (Wang et al., 2020; Rahman et al., 2020).

Monitoring the number of microplastics is a demanding job that requires identifying and picking out microplastics at low concentrations from all-inclusive water samples (e.g., minerals, organic particles, the additive and pigment chemicals). Some efforts have been put into extracting microplastic particles by density separation (Strungaru et al., 2019), removing biogenic material with chemicals such as a proteolytic enzyme (Cole et al., 2014) or hydrogen peroxide solution (Nuelle et al., 2014). Without such sample pretreatment methods, the ideal pipeline would be a combination of physical characterization by microscopy, and chemical characterization by spectroscopy or thermal analysis (Shim et al., 2017). Despite of their advantages in determining chemical compositions and decreasing false positive rates, vibrational spectroscopic techniques are usually time and cost consuming, including (Shim et al., 2017; Hidalgo-Ruz et al., 2012): FTIR (Fourier-transform Infrared) Spectroscopy (Simon et al., 2018; Primpke et al., 2017), Raman Spectroscopy (Van Cauwenberghe et al., 2013; Anger et al., 2019) and EDS (Energy Dispersive X-ray Spectrometry) (Wang et al., 2017). Meanwhile, as a destructive method, thermal analytical techniques prevent further analysis of samples (Shim et al., 2017).

Physical characterization, though simple and fast, suffers from high false positive rates due to the lack of chemical information. Microplastics picking is primitively done by visual identification, or with the aid of visible light microscopy (VLM) (Wang et al., 2017; Song et al., 2015). However, visual screening is a labour-intensive task for experts and trained volunteers. Besides, false identification rate is high, especially for small and transparent particles (over 70% (Shim et al., 2017)). Compared to visual identification and VLM, scanning electron microscopy (SEM) has the following advantages: (1) SEM provides a much greater depth of field than VLM. (2) SEM can offer more clear and higher resolution details of surface textures for further discrimination, despite the loss of colour information. Also, it has the potential to go down to the scale of nanoplastics (The best image resolution of the SEM we used was 1 nm). (3) SEM permits further analysis with EDS to obtain elemental composition signatures in the case where morphology alone is unable to identify microplastics. Meanwhile, various advanced microscopic automation techniques (Rudnaya et al., 2010; Schorb et al., 2019) encourage high-throughput data collection and help produce micrographs in a faster and cheaper way.

The physical morphology and chemical composition of observed plastic debris may vary significantly according to the methods by which polymeric materials are manufactured and degraded. On one hand, microplastics can be classified based on their chemical compositions. Though varying from region to region, the following categories contribute the most to the plastic pollution (Lusher et al., 2014; Lusher et al., 2015; do Sul and Costa, 2014; Eerkes-Medrano et al., 2015; Strungaru et al., 2019; Digka et al., 2018; Sait et al., 2021): polyethylene (PE), polyethylene terephthalate (PET), polystyrene (PS), polyurethane (PUR), polycarbonate (PC), polypropylene (PP), polyacrylonitrile (PAN), polyamide (PA, Nylon) and polyvinyl chloride (PVC). Fig. 1 shows the examples of SEM images of microplastics in different chemical compositions collected from daily supplies.

On the other hand, microplastics can be classified into five categories based on their shapes (Lusher et al., 2014; do Sul and Costa, 2014; Wagner et al., 2014; Free et al., 2014): fibre/line, bead/pellet, fragment, film and foam, as shown in Fig. 1. Here virgin resin pellets and microbeads are combined into one category to represent hard and rounded plastic particles (Free et al., 2014). The shapes of microplastics with the same chemical composition may vary a lot due to different courses of manufacturing and degradation. Meanwhile, it is difficult to distinguish materials in the same shapes and different chemical compositions without chemical characterization (e.g., synthetic fibres and natural fibres as cotton). Nevertheless, it is still possible to classify objects in SEM images based on their shapes and structures (Aversa et al., 2018) in high accuracy, thanks to the surging image processing techniques in recent years with in-depth research on artificial intelligence and self-driving techniques. In our work, we built the SEM image dataset of microplastics in different shapes and chemical compositions. Since the concentration of microplastics in environmental samples is too low, our samples were collected from daily supplies listed in Table 1. More concentrated microplastics with pure forms help to establish a comprehensive dataset of various microplastics. We hope in the future, the growing datasets with more and more detailed morphological information provided by the advanced microscopes could make it possible to automatically identify and quantify the microplastics in environmental samples, therefore, to help us monitor the microplastic pollution.

In all, the aim of this work is to use computer vision and deep learning techniques to facilitate microplastics quantification, and further to monitor the microplastic pollution in the ecosystem. The main contributions are summarized as below: (1) we have collected microplastics in different shapes and chemical compositions from daily supplies and imaged them by SEM. (2) we have built the first labelled SEM dataset of microplastics for image segmentation to our best knowledge. (3) we have applied deep learning methods to automate and facilitate quantification and classification of microplastics in SEM images, and compared the performance with traditional methods. The paper is organized as follows. Section 2 illustrates the methods used in SEM experiments, dataset creation, semantic and instance segmentation, and microplastics classification. Section 3 demonstrates the results of microplastic segmentation, quantification and classification and compares the performance of deep learning approaches and conventional methods. Finally, a further discussion and conclusion are given in Section 4.

2. Methodology

2.1. Experimental details

Though microplastics can be observed by VLM, SEM could provide a greater depth and finer surface details to prevent false identification for small and transparent microplastics. Electron micrographs were obtained using three different scanning electron microscopes, i.e., Hitachi SU3500, Hitachi SU5000, and Hitachi SU8230, located in the Open Center for the Characterization of Advanced Materials (OCCAM) at the University of Toronto.

2.1.1. Samples

Typically, samples collected directly from water bodies have very diluted amounts of microplastics. For example, the concentration in the Arctic is 38–234 items/m^3 (Wang et al., 2020). An important source of microplastics is sewage-contaminated by fibres from washing clothes (Browne et al., 2011). Evaluation of microplastics from sediments showed that the polyester and acrylic fibres used in clothing resembled those found in environments that received sewage discharges and sewage effluent. Sampling wastewater from domestic washing machines demonstrated that a single garment could produce greater than 1900 fibres per wash (Browne et al., 2011). This suggests that a large proportion of microplastics fibres found in the marine environment may be derived from sewage as a consequence of washing clothes. For this reason, in this study, laundry water samples were collected by doing laundry to obtain relatively clean water samples with pieces of microplastics. 50 ml water samples with 100% polyester were gathered after doing one laundry wash with just a drop of SpringTime Complete detergent. Microplastics of other types were also obtained by cutting, cracking, and grinding larger pieces from

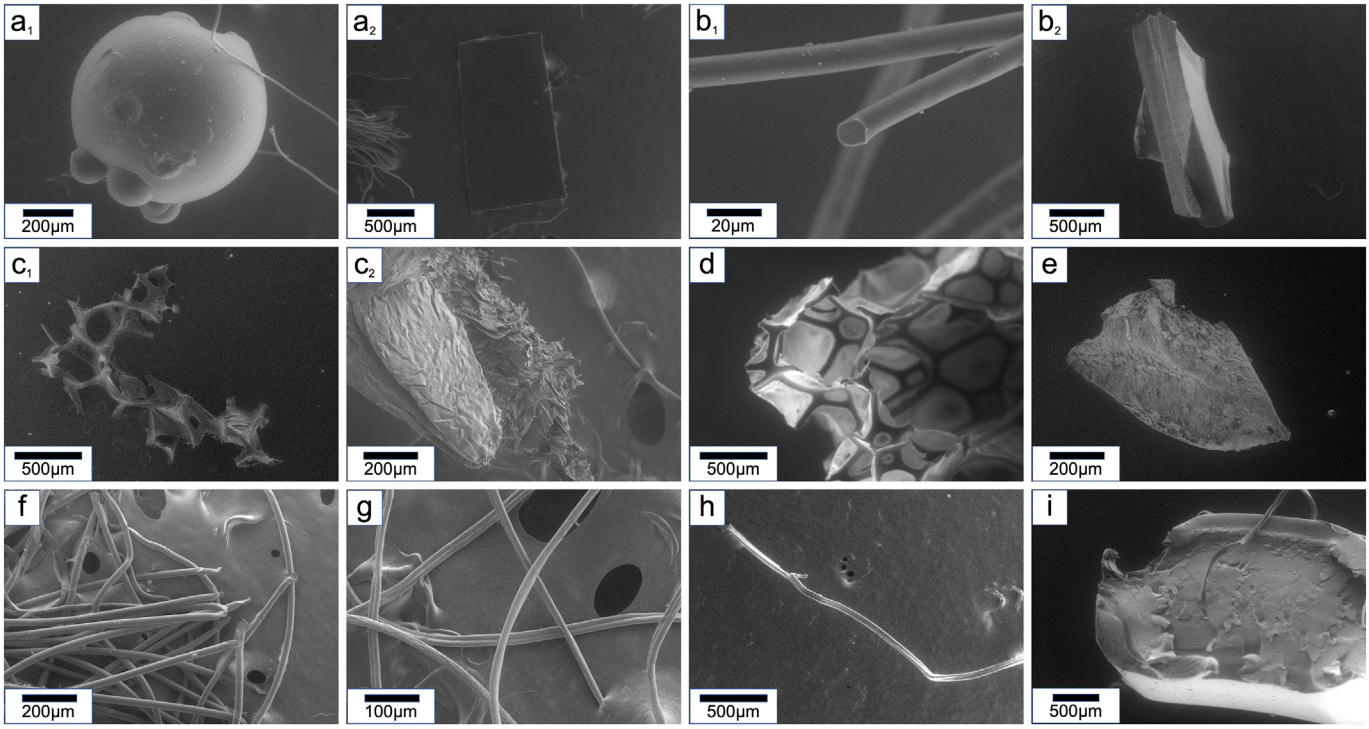

Fig. 1. Microplastics in different chemical compositions and shapes: (a) PE bead/film, (b) PET fibre/fragment, (c) PS fragment/foam, (d) PUR foam, (e) PC fragment, (f) PP fibre, (g) PAN fibre, (h) PA fibre, (i) PVC fragment.

plastic products. The samples used for visualising microplastics in different shapes and types in Fig. 1 are summarized in Table 1.

2.1.2. Samples preparation

Dry microplastics samples were obtained directly from plastic sources and then placed on top of a double-sided adhesive carbon or copper tape attached to an SEM sample holder using tweezers. Water samples were air-dried, or heat dried by placing samples in a 50 ml beaker on top of a hotplate and heating samples for approximate 30 min until less than a millilitre of water was remaining. To accelerate the evaporating process, PS was suspended by isopropyl alcohol instead of water. A silicon wafer was used as a substrate to enhance the contrast in SEM images. Each silicon substrate is about $1cm^2$ in area. Each wafer was cleaned with a Kimwipe using deionized water, then methanol, and then left to air dry. 10 μl wet sample was pipetted onto a cleaned silicon wafer and was left to air dry. Each silicon substrate was carbon taped at the bottom and hot glued at opposing corners onto a sample holder as shown in Fig. 2.

2.1.3. Charging reduction

Given that microplastics are non-conductive, charging effects will severely distort SEM images, especially for small objects in high magnification. The methods to reduce charging effects include (Goldstein et al., 2018): coating (Joy and Joy, 1996), adjusting acceleration voltage (Burnstock and Jones, 2000), using low vacuum mode, reducing beam current, increasing scan speed, sample tilt angle adjustment. Most of the particles in this paper are taken in the range of 50 μm–1 mm. Diameters of both natural and synthetic fibres lie between 7 and 20 μm as shown in Figs. 1-b1 and 3-a2. Most of the fibre samples were imaged on copper tape to aid in alleviating the charging effects. Environmental scanning electron microscopy and low-voltage scanning electron microscopy were used. Coating the samples with carbon or metal was avoided in order to capture the surface features of the samples. Some samples on the carbon tapes were in the low vacuum mode at around 40 Pa. The accelerating voltage varied between 1 and 3 keV. Further investigation into imaging insulating materials can help improve future work.

Table 1
Microplastics samples sources.

Composition	Shapes	Sources
PE	Bead/film	Face wash, HDPE from inflatable packing film
PET	Fibre/fragment	Washing/dryer machine, shampoo bottle, sewing kit thread
PS	Fragment/foam	Foam cup/wiper, packing Styrofoam, lunch box
PU	Foam	Cookware scrubber
PC	Fragment	Safety goggle
PP	Fibre	Surgery mask
PAN	Fibre	Acrylic fibre
PA	Fibre	Carpet
PVC	Fragment	PVC pipe

2.2. Dataset creation

A manually labelled SEM dataset of microplastics was built. Image segmentation and shape classification were performed on 3 classes: fibres, beads and fragments as shown in Fig. 3 since only a few images of films and foams were taken. The distribution of microplastics is summarized in Table 2.

Fibres and fragments are the major shapes of microplastics existing in the natural environment (Wagner et al., 2014; Naji et al., 2018). The majority of microplastics labelled are microplastics fibres (MPFs) since MPFs contribute most to the microplastic pollution in the marine environment (Desforges et al., 2014; Lusher et al., 2014; Lusher et al., 2015; do Sul and Costa, 2014; Sait et al., 2021), ranging from 68% to 95.9%. For image segmentation, fibres are thin (7–20 μm) and elongated curvilinear objects which are more difficult to be extracted from images than particles (fragments or beads). Most of the SEM images have dimensions 1280 × 960 with scale bars at the bottom while some are 2560 × 1920. In all experiments with mixed datasets (Experiment #1 semantic segmentation, Experiment #4 shape classification), micrographs were directly resized to 512 × 512 during the training and reverted to their original image dimension after the training. For experiments trained and tested on single sub-datasets (Experiment #2 semantic segmentation, Experiment #3 fibre instance

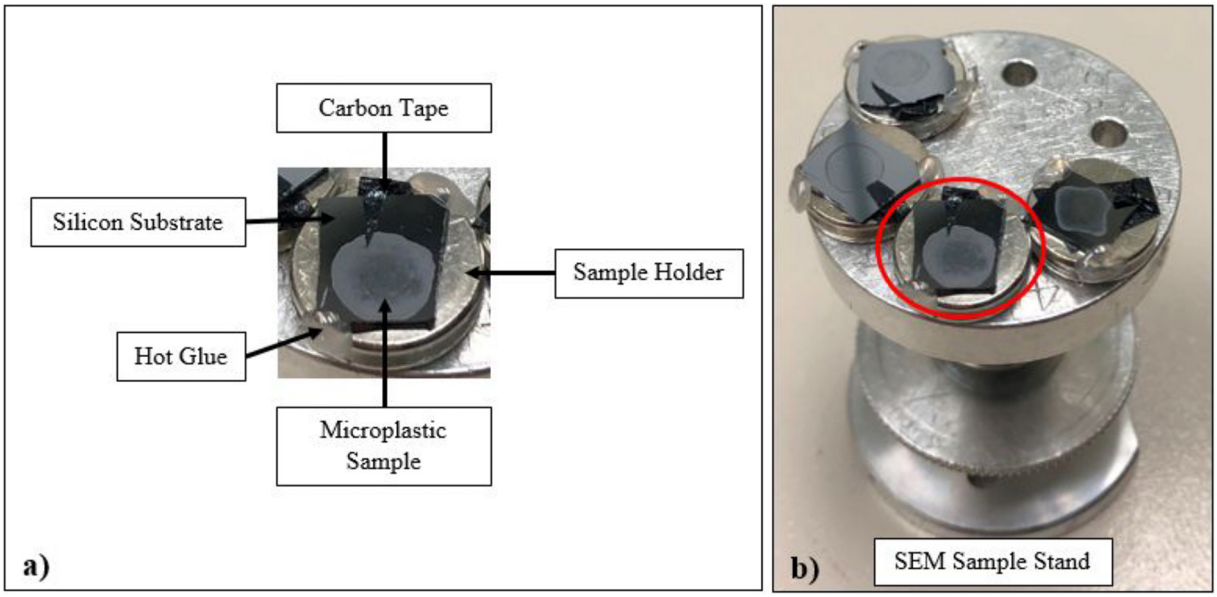

Fig. 2. Sample preparation: (a) silicon substrate mounting configuration on sample holder; (b) an example of sample holder arranged on an SEM sample stand.

segmentation), micrographs of MPFs were split into a patch of two 512 × 512 or four to increase the number of available samples for training and to eliminate the effects of resizing on thin MPFs. Ground-truth segmentations were labelled manually by ImageJ and other image processing software. It took more than half an hour to label a micrograph with multiple MPFs or porous fragments.

The fibre dataset was split into two parts. In *fibre_1* (Fig. 3-a1), 41 images were collected from single experiments with clean background. An additional 49 images in *fibre_2* (Fig. 3-a2) were obtained in many other different experiment settings to improve the generalization ability of the trained models. For the same reason, fragment (*fragment_1* in Fig. 3-c1 and *fragment_2* in Fig. 3-c2) and bead datasets were acquired in different settings. Moreover, 101 and 100 images were cropped from *fibre_1* and *fibre_2* respectively to constitute the datasets *fibre_1crop* and *fibre_2crop* for Experiment #2. Each fibre in *fibre_1crop* was also labelled in different colours and saved in the forms of label map, indexed png and VGG Image Annotator (for Mask-RCNN training) for instance segmentation. The numbers of microplastics in each micrograph were documented in dataset1 and in Table 2 expect for *fibre_2/fibre_2crop* since fibres in this dataset are too tangled and crowded for humans to quantify. The complete training dataset of semantic segmentation and shape classification is open for download (dataset1) as well as the dataset for instance segmentation (dataset2). The experiment setting for each micrograph was recorded and uploaded together with the original SEM micrographs, full-size segmentations (dataset3) and major results (result).

2.3. Segmentation

Image segmentation is an image transformation problem to partition a digital image into multiple segments, which facilitates further analysis. After years of efforts, various non-learning based methods have been successfully utilized in image segmentation, including (De et al., 2016)

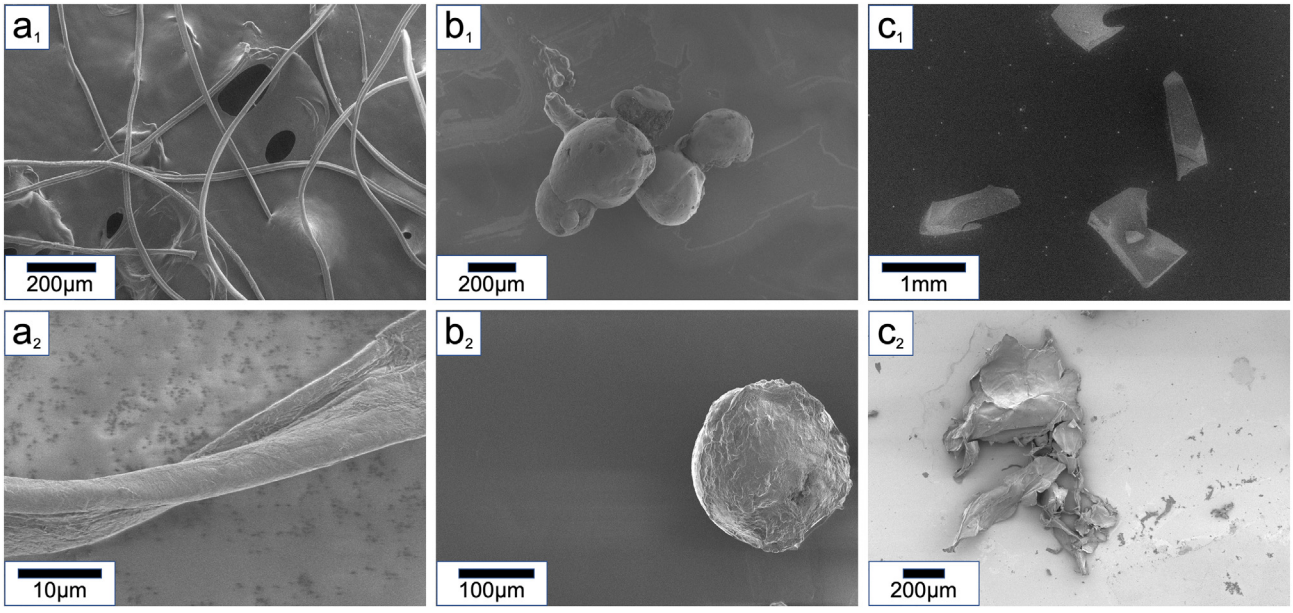

Fig. 3. Microplastics samples in the dataset: (a) fibre, (b) bead, (c) fragment.

Table 2
Microplastics SEM image dataset.

MP shapes	Datasets	Compositions	# of images	# of MPs
Fibre	*fibre_1 (fibre_1crop)*	PET	41 (101)	248 (604)
	fibre_2 (fibre_2crop)	PET, PAN, PP	49 (100)	– (–)
Bead	*bead*	Copolymer in body wash	51	69
Fragment	*fragment_1*	PC, PS	55	97
	fragment_2	PS	41	61

histogram thresholding methods (Otsu (Otsu, 1979), adaptive, Niblack, Sauvola (Sauvola and Pietikäinen, 2000)), boundary-based methods (image processing operators, edge detection), region-based methods (watershed, region growing), mathematical morphology, normalised cut, etc. However, images taken from different devices in different fields have widely divergent features. The complexities make it challenging to find a one-size-fits-all approach due to the difficulties of translating domain knowledge into machine language. Some examples for non-learning based methods used in quantifying microplastics include SEM (TUM-Particle Typer (von der Esch et al., 2020)), Raman Spectroscopy (Anger et al., 2019), FTIR (Simon et al., 2018; Primpke et al., 2017) and staining dye solution (using software MP-VAT (Prata et al., 2019)). Most of the aforementioned methods are all based on closed-source software or thresholding methods.

Learning-based methods is surging in recent years, especially deep learning. Domain knowledge is incorporated into training datasets with experts providing ground-truth segmentations. Afterwards, one can also resort to various deep learning architectures for image segmentation, including (Minaee et al., 2021) convolutional neural net (CNN), recurrent neural net (RNN), long short-term memory (LSTM), encoder-decoder, generative adversarial network (GAN). The representative models include FCN (Long et al., 2015), SegNet (Badrinarayanan et al., 2017), U-Net (Ronneberger et al., 2015), FPN (Lin et al., 2017), Mask-RCNN (He et al., 2017), DeepLab (Chen et al., 2017), etc. Among all these approaches, U-Net and its variants (Siddique et al., 2021) have shown great success in dealing with medical images with just a few ground-truth segmentations. Though deep learning approaches have been widely used in microscopy images ((Xing et al., 2017), EM-net (Khadangi et al., 2021), CDeep3M (Haberl et al., 2018; Matuszewski and Sintorn, 2019)), they have only a few applications in microplastics analysis. Deep pixel embedding was used to separate tangled fibres in (Wegmayr et al., 2020) which achieved a better performance than Mask-RCNN. In (Lorenzo-Navarro et al., 2021), a large image was split into overlapped patches, segmented by U-Net and then concatenated into the final result.

Our work differs from previous work in that microplastics imaged by SEM, in general, have higher magnifications and show more microscopic details than those by VLM. Meanwhile, they also pose some challenges for further analysis: (1) MPFs are elongated, may overlap or exceed the image's borders as shown in Figs. 1-b1 and 3-a2. Meanwhile, MPFs in the datasets have non-uniform lengths, widths, curvatures and textures. (2) Unlike microplastics on A4 paper photographed by VLM (Lorenzo-Navarro et al., 2021), SEM micrographs show more details of substrate and contamination information. (3) Electron micrographs may be distorted by astigmatism, sample charging, aberrations, etc. Problem (1) implies that object detection methods including the bounding box methods used in (Lorenzo-Navarro et al., 2021; Dalal and Triggs, 2005) are not appropriate for images of MPFs or images containing only a few large particles. Problems (2) and (3) limit the application of thresholding methods and make it more labour-intensive to obtain the ground-truth labels. Both U-Net (Ronneberger et al., 2015) and its variant MultiResUNet (Ibtehaz and Rahman, 2020) were used for semantic segmentation. U-Net was further combined with object-aware pixel embedding (Chen et al., 2019) for instance segmentation to pick out every single fibre instance from tangled fibres, therefore to facilitates counting of fibres. Data augmentation (Ronneberger et al., 2015) was carried out to increase the amount of data in all the segmentation tasks.

2.4. Classification

Though it is difficult to identify microplastics with different chemical compositions from a small number of micrographs, classifying microplastics based on their shapes and appearance has been implemented by SVM (Support Vector Machine), decision tree, KNN (K Nearest-Neighbor), and bagging (random forest) or boosting (AdaBoost) algorithms in (Lorenzo-Navarro et al., 2020; Lorenzo-Navarro et al., 2018). Transfer learning has proved its success to transfer knowledge in optical images to the domain of scanning electron micrographs (Aversa et al., 2018). Various deep learning models were learnt and compared including MLP, CNN, HC-CNN (Zhu et al., 2020) and other models based on VGG16 (Simonyan and Zisserman, n.d.; Lorenzo-Navarro et al., 2021) or ResNet (He et al., 2016).

A deep learning model was trained in this paper to demonstrate that deep learning could be also utilized in microplastics shape classification from SEM micrographs. Due to the limited performance of from-scratch trained model from this small SEM microplastics dataset, a VGG16 architecture was adapted in our model: the weights of the convolutional layers were pre-trained on ImageNet and fixed; a fully-connected (FC) layer with 64 units; a FC layer with 32 units followed by a dropout layer with a dropout rate 0.2; a FC layer with 3 units followed by a softmax activation function to output the probabilities that an image belongs to each category. The number of units in FC layers was reduced to prevent over-fitting and images were resized to 224 × 224. The present classification network is independent of the segmentation. However, it can be incorporated into a multi-class instance segmentation network in future work to deal with the practical situation when microplastics in different shapes and chemical compositions appear in the same SEM image. The overall architecture is shown in the graphical abstract.

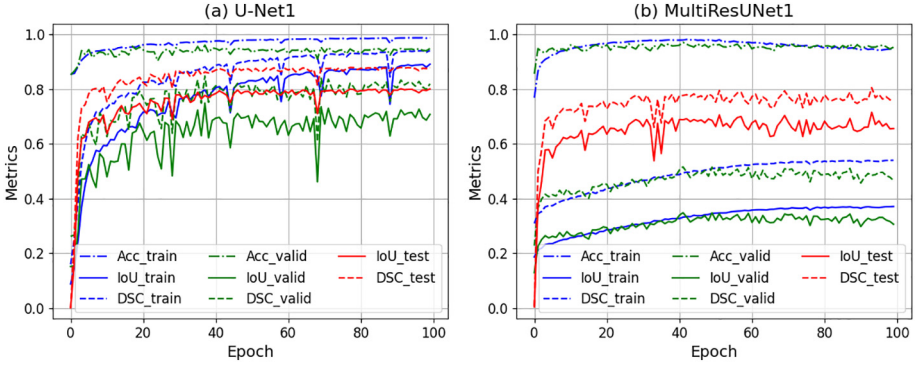

Fig. 4. Progress of the training (blue), validation (green) and testing (red) performance of models with the number of epochs. Accuracy (dash dot lines), IoU (solid lines) and DSC (dash lines) were used as evaluation metrics.

Table 3
Results of microplastics segmentation using U-Net and MultiResUNet on the full dataset.

		U-Net1	U-Net2	MultiResUNet1	MultiResUNet2
	# of paras	7,759,521	31,030,593	7,262,504	29,061,741
Datasets	Fold	IoU/DSC (%)	IoU/DSC (%)	IoU/DSC (%)	IoU/DSC (%)
Full	1	79.57/87.55	80.57/88.26	73.71/82.51	74.99/84.19
	2	80.13/87.98	81.27/88.72	71.52/80.53	77.18/85.39
	3	74.30/83.79	73.76/83.34	73.30/83.38	75.62/85.11
	4	77.90/86.64	80.18/88.24	75.82/84.95	76.08/85.10
	5	80.60/88.39	81.85/89.30	75.95/84.29	80.20/87.95
	Avg. (Best)	**78.50 ± 2.56/ 86.87 ± 1.84**	**79.53 ± 3.29/ 87.57 ± 2.40**	**74.06 ± 1.86/ 83.13 ± 1.72**	**76.82 ± 2.05/ 85.55 ± 1.42**
Fibre	Avg.	72.48/83.02	73.89/84.05	62.44/75.76	66.07/78.69
	fibre_1 Avg.	84.46/91.29	85.77/92.10	72.26/83.73	74.90/85.45
	fibre_2 Avg.	62.45/76.11	63.95/77.32	54.22/69.09	58.67/73.03
Bead	Avg.	78.25/85.98	78.96/86.59	82.10/88.83	81.69/88.58
Fragment	Avg.	81.67/88.99	82.26/89.28	66.98/76.82	75.37/83.74
	frag._1 Avg.	88.60/93.42	89.77/94.25	81.49/88.95	88.26/93.38
	frag._2 Avg.	72.37/83.05	72.19/82.61	47.51/60.53	58.07/70.82
Full	**Avg. (Last)**	**77.44/86.08**	**78.37/86.71**	**68.51/79.00**	**73.20/82.87**

3. Experiments and results

Different algorithms had been implemented and compared for semantic segmentation, instance segmentation and shape classification of microplastics SEM images.

3.1. Microplastics SEM image semantic segmentation results

To quantify microplastics, semantic segmentation was performed to extract the microplastics of interest from other materials in the background including the substrate, minerals, chemicals, organic matters, and organisms. Two metrics have been used to evaluate the performance of image segmentation: Intersection over Union (IoU or Jaccard index) and Dice Similarity Coefficient (DSC). They range from 0 to 1 and reach the maximum when ground-truth segmentation and the predicted one completely overlap. Both were converted to percentage ratios for better readability. Four significant figures were kept for values calculated from different metrics since their difference might be smaller than 0.1%. Accordingly, the calculated deviations were kept in the same accuracy (0.01%).

3.1.1. Experiment #1

Semantic segmentation was performed on the full dataset and Fig. 4 shows the progress of the training, validation and testing performance with the number of epochs. The numbers of filters in the original U-Net (U-Net2) and MultiResUNet (MultiResUNet1) were (64,128,256,512,1024) and (32,64,128,256,512), respectively. To make these two models comparable (with the similar numbers of trainable parameters), U-Net1 (32,64,128,256,512) and MultiResUNet2 (64,128,256,512,1024) were implemented. In all four cases, the testing performance was better than that of training and validation at the beginning since: U-Net has dropout layers with large dropout rates (0.5); MultiResUNet uses BN (Batch Normalisation) layers. The testing metrics no longer increase after 50 epochs. All the following experiments were trained for 50 epochs with smaller models (U-Net1 and MultiResUNet1) on 12G and 16G GPU clusters (Graham) with the support of Compute Canada.

A 5-fold cross-validation was carried out: the whole dataset was randomly split into five mutually exclusive parts; each time, images in four folders served as training samples with a 10% split for validation, and images in the last one folder served as test samples. The results are organized in Table 3. The upper part shows the results of each fold where the best result among all epochs was collected. The lower part shows results of each type of microplastics where the results from the 100th epochs were collected. The performance improved with more filters and parameters. Moreover, the performance depends heavily on the dataset: both models achieve better results (IoU > 70%) on the homogeneous datasets which contain similar images with clean background, e.g., *fibre_1*, *bead*, *fragment_1*; the scores fall on the datasets in which images have diverse features at different scales, e.g., *fibre_2*, *fragment_2*. We also train each sub-dataset of microplastics with the same chemical composition separately and both models have a significant improvement on the performance shown in Table 4. The values for U-Net and MultiResUNet were calculated by 5-fold cross-validation, which trained 5 models, then calculated the average scores and standard deviation. The values of non-learning based thresholding methods just take the average scores over all images.

It can be concluded that with similar numbers of trainable parameters, U-Net has a better performance than MultiResUNet on a compound dataset. However, for a more homogeneous dataset, MultiResUNet has a slight advantage over U-Net, which is consistent with the results of SEM images in (Ibtehaz and Rahman, 2020). These two deep learning models all precede the thresholding-based methods.

3.1.2. Experiment #2

U-Net and MultiResUNet have been trained on individual sub-dataset with the same shapes and compared with non-learning based thresholding methods for semantic segmentation. As shown in Table 4, U-Net and

Table 4
Results of microplastics segmentation on sub-datasets. Deep learning methods outmatch Otsu's method on different datasets. The standard deviations are given for all 5-fold averages.

	U-Net1	MultiResUNet1	Otsu
Datasets	IoU/DSC (%)	IoU/DSC (%)	IoU/DSC (%)
Fibre_full	78.49 ± 1.86/87.49 ± 1.16	**78.80 ± 2.36/87.55 ± 1.75**	45.47/60.99
Fibre_1crop	86.74 ± 2.14/92.80 ± 1.33	**87.23 ± 1.61/93.06 ± 1.04**	54.38/70.24
Fibre_2crop	73.28 ± 3.49/83.94 ± 2.63	**74.30 ± 2.87/84.74 ± 1.99**	37.26/52.52
Bead	93.08 ± 0.62/96.27 ± 0.27	**93.56 ± 1.89/96.55 ± 1.05**	23.98/35.70
Frag._full	**84.14 ± 1.81/90.86 ± 1.21**	76.72 ± 8.17/85.32 ± 6.70	–
Frag._1	92.73 ± 2.17/96.07 ± 1.27	**93.11 ± 1.93/96.29 ± 1.10**	63.70/72.09
Frag._2	75.33 ± 5.35/85.39 ± 4.07	**78.22 ± 4.22/87.38 ± 3.03**	46.70/62.03

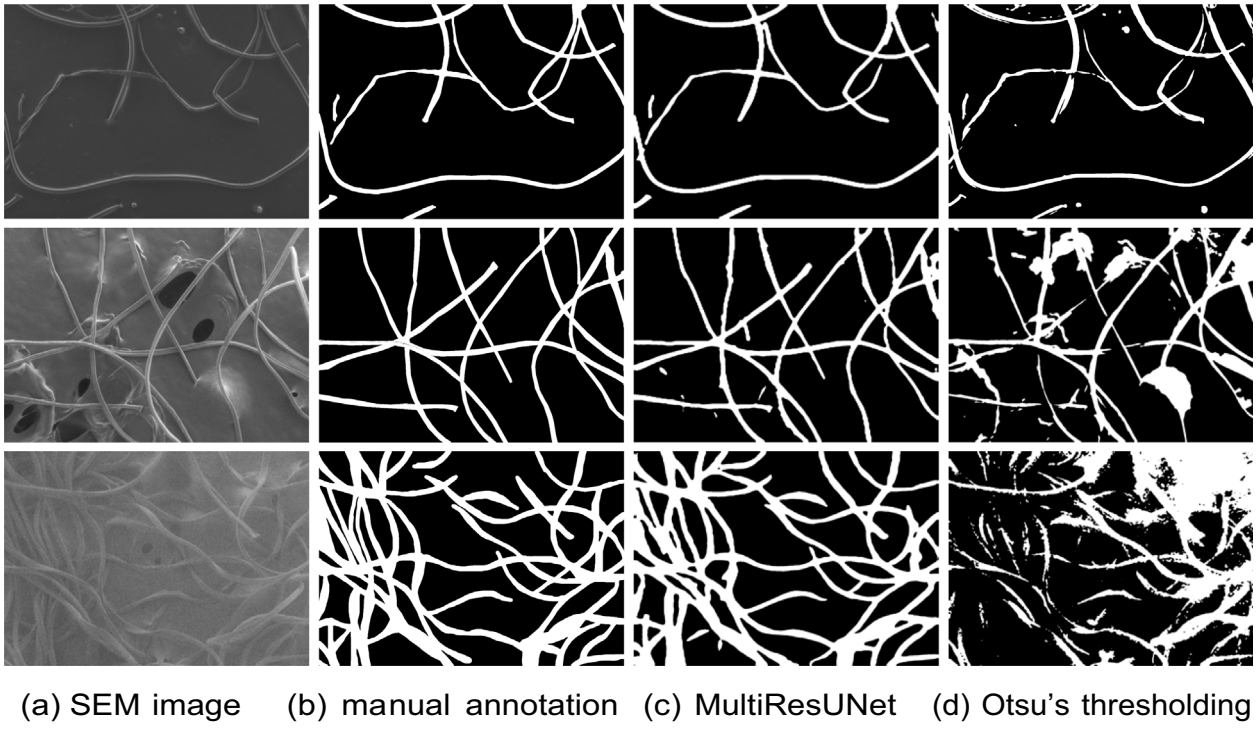

Fig. 5. Results on fibres (IoU/DSC%). Top: with clean background (c) 86.10/92.53, (d) 56.78/72.43. Middle: with charging and holes (c) 84.95/91.86, (d) 46.06/63.07. Bottom: in low SNRs (c) 82.39/90.34, (d) 35.06/54.42.

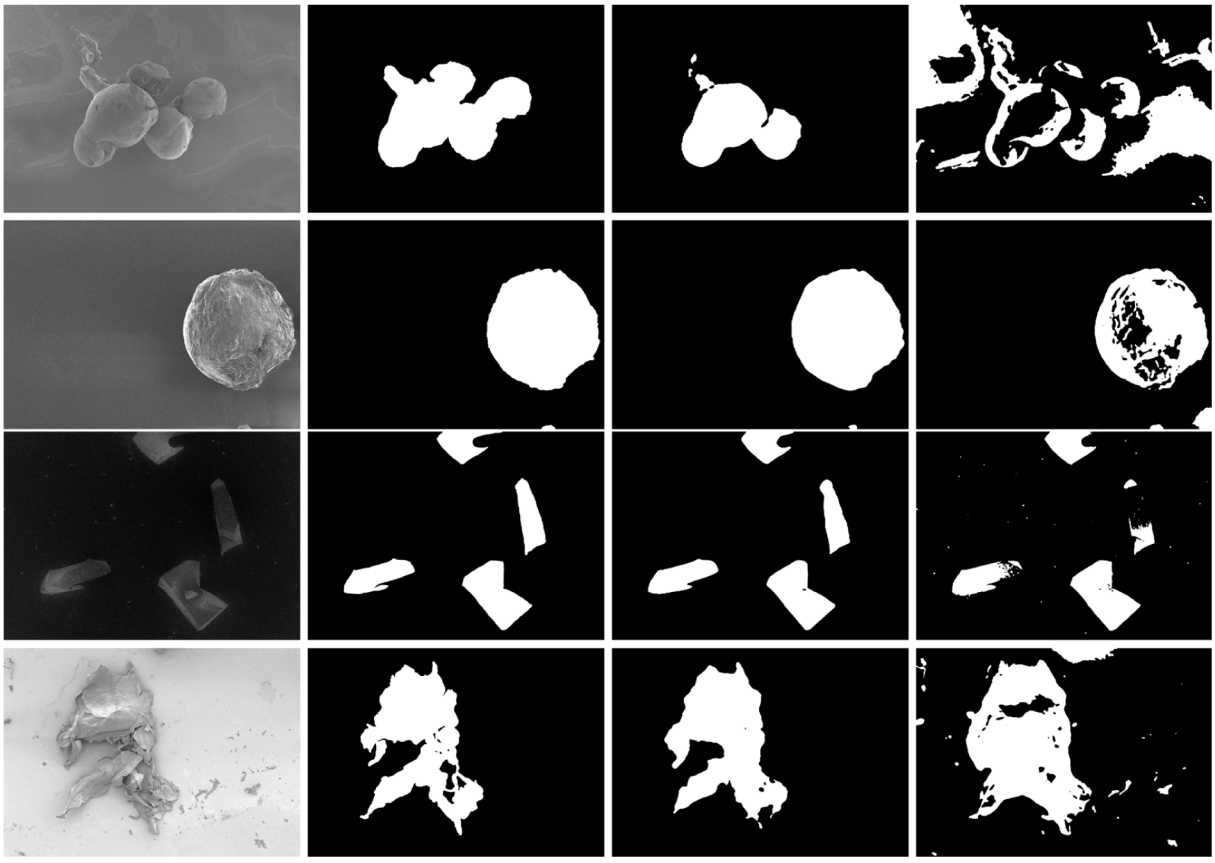

Fig. 6. Results on beads and fragments (IoU/DSC%). From top to bottom, Bead 1: (c) 65.03/78.81, (d) 21.38/35.23. Bead 2: (c) 98.23/99.11, (d) 74.67/85.50. Fragment 1: (c) 95.45/97.67, (d) 80.29/89.07. Fragment 2: (c) 86.03/92.49, (d) 59.08/74.28.

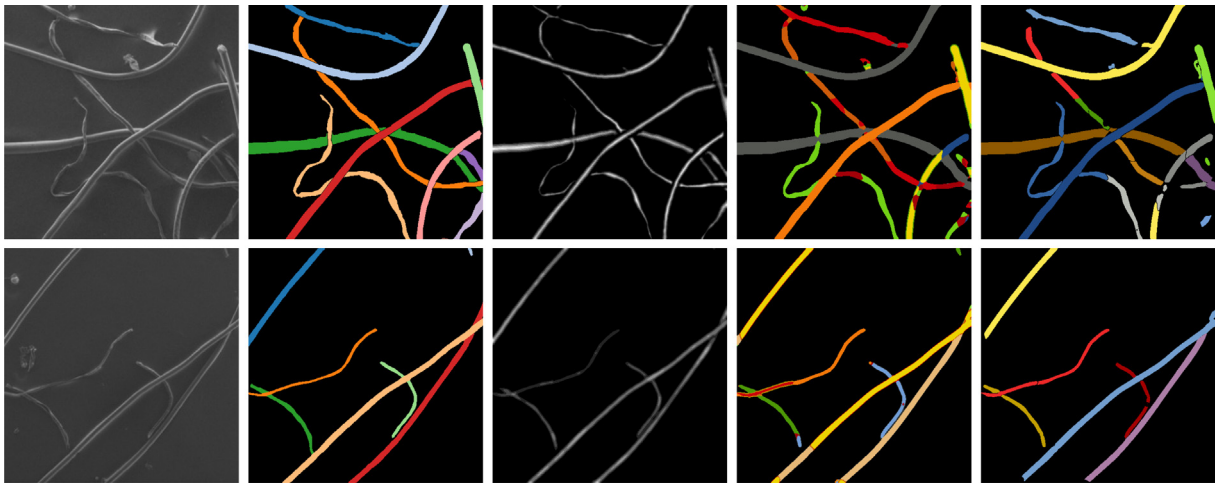

Fig. 7. Instance segmentation results on fibre_1 datasets. (d) Mean-shift and (e) a heuristic method were used for postprocessing. Different instances were labelled in different colours for counting.

MultiResUNet have comparable performances, and both are better than Otsu's thresholding methods. The results of fibres, beads and fragments are shown in Figs. 5, 6, respectively. IoU and Dice coefficients scores are given in percentage for each prediction. U-Net and MultiResUNet have similar performance and predicted segmentations. For *fibre_1* and *fibre_2*, a Gaussian blur was performed followed by Otsu's thresholding. The kernel size of Gaussian smoothing is 13 × 13 calculated by the line search. For *bead*, *fragment_1* and *fragment_2*, the kernel sizes are 27 × 27, 27 × 27 and 23 × 23, respectively. For *fragment_2*, binarized segmentation was reversed since the background has a higher intensity than particles. The overall metrics for Otsu's methods are not calculated due to the various kernel sizes.

3.2. Microplastics instance segmentation and quantification results

The numbers of microplastics are often reported by the community to quantify their concentration at different sites. However, semantic segmentation is not adequate to report the number for touching, overlapping or densely packed microplastics, especially for tangled fibres. As a more advanced task, instance segmentation has been implemented on electron micrographs with overlapping particles EMPS datasets (Yildirim and Cole, 2021). In our work, instance segmentation was performed on fibre datasets not only to extract fibres from the background but also to separate different instances of fibres and therefore to determine the numbers in each micrograph.

Since a lot of micrographs in fragment and bead datasets contain only one particle, instance segmentation was done only for fibre datasets as shown in Fig. 7. Due to the large microplastics-to-background ratios in SEM images, bounding boxes are of large size and overlap a lot, especially for fibres. Mask-RCNN was problematic to detect multiple objects from the shared bounding boxes and to generate accurate masks in our experiment. Fortunately, pixel embedding has shown its success in instance segmentation (Kong and Fowlkes, 2018; Chen et al., 2019; Wegmayr et al., 2020). Each pixel was regressed into a hyper embedding space so that pixels from the same instance have a higher cosine similarity (Kong and Fowlkes, 2018). We adopted the network (Chen et al., 2019) with a double-headed U-Net backbone network for instance segmentation. The expansive path consists of the distance regression branch and the embedding branch. The former predicts the distance map while the latter predicts the object-aware embedding vector for each pixel. Pixels in the same instance have small cosine distances, therefore the instance to which a pixel belongs can be inferred from its embedding vector.

3.2.1. Experiment #3

16-dimensional embedding space was used in our experiments. The number of instances in the image can be determined by the number of clusters in the embedding space. Results from two postprocessing methods are shown in Fig. 7: meanshift and a heuristic method. Meanshift determined the number of clusters based on the bandwidth estimated from the image. However, close points in the embedding space might be far in pixels with an imperfect estimation of embedding vectors. A heuristic method (Chen et al., 2019) was also used: given seeds calculated from local maximums, nearby pixels with close embedding vector were incorporated into the group. An additional combination step was used when neighboring regions have high cosine similarities. The total number of fibres is 161 among 21 testing images, which is comparable to the ground-truth value of 112. The overestimation is mainly caused by inaccurate embedding vectors, which might be alleviated with more training datasets. More results are available in result.zip. The instance segmentation framework using U-Net with pixel embedding is promising to quantify microplastics even if they are densely packed and tangled. More precise embedding vector estimation is expected in future work given more finely labelled datasets.

3.3. Microplastics shape classification results

3.3.1. Experiment #4

A 5-fold cross-validation was carried out. A VGG16 model with fine-tuned FC layers was trained on the augmented dataset. An Adam optimizer was used (learning rate = 10^{-4}, batch size = 8). An early stop was carried out if the validation loss does not improve in 5 epochs. The performance is shown in Table 5. Overall, the network predicted shape labels accurately (accuracy = 98.33%). However, more SEM images are expected to be taken and included in classification in future work.

Table 5
Results of shape classification using transfer learning.

Fold	Accuracy (weighted recall)	Weighted precision	Weighted F1	# of epochs
1	97.98%	98.07%	97.89%	13
2	100.0%	100.0%	100.0%	18
3	95.65%	96.07%	95.63%	11
4	100.0%	100.0%	100.0%	13
5	98.04%	98.13%	98.02%	21
Average	98.33 ± 1.80%	98.45 ± 1.64%	98.31 ± 1.81%	15.20 ± 4.15

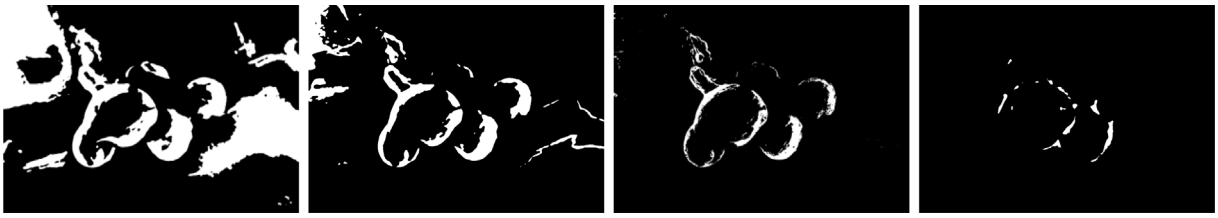

Fig. 8. Results of thresholding methods with different parameters (IoU/DSC%): (a) Otsu's threshold with a 27 × 27 Gaussian blur; (b) fine-tuned threshold of (a); (c) Otsu's threshold with a 3 × 3 Gaussian blur; (d) Sauvola thresholding with a window size 101 × 101.

4. Discussion

In this work, deep learning models were trained for image segmentation and shape classification of microplastics imaged by scanning electron microscopes. On one hand, the VGG16 model with pre-trained convolutional layers and fine-tuned FC layers can achieve high shape classification scores (accuracy = 98.33%). On the other hand, the quantification task requires microplastics to be extracted from micrographs, which are extremely labour-intensive. Two deep learning models, U-Net and MultiResUNet were trained on microplastics in different shapes: fibres, fragments, and beads. Both models trained on individual folders achieve satisfactory results (IoU > 70%), and both models get over 85% IoU on *bead*, *fragment_1*, and *fibre_1* datasets. Both models significantly outperform conventional image processing techniques. U-Net was also combined with object-aware pixel embedding to perform instance segmentation and therefore to count the number of fibres. The training time for image segmentation lies between 1 and 9 h depending on the number of parameters and the size of images since it takes a longer time to calculate the metrics for a larger image. With trained models, it takes only seconds to segment a new micrograph. For comparison, the average time is approximately half an hour per micrograph for manual annotations. Deep learning accelerates the quantification of microplastics to a great extent, especially in the case when the microplastics are densely packed or are imaged in complex environments and poor experimental settings, as shown in Fig. 5.

In the image segmentation on the full dataset, images were directly resized to 512 × 512, which might miss lots of details to infer full-size predictions using interpolation. For example, thin fibres only take up several pixels. Otsu's method was chosen as the baseline for comparison. As a non-learning based global thresholding method, the result is sensitive to the threshold and other parameters. For example, fine-tuning the threshold may benefit the single image in Fig. 8-b, but not for the entire dataset. Javier (Lorenzo-Navarro et al., 2021) used Sauvola, a local thresholding method as the baseline, which was designed for document image binarization. Their samples were small compared to the whole image and were arranged on a white A4 paper which resembled words on documents. Since electrons were shined on the samples uniformly, there were no significant changes in global illumination. Rather than improving the performance, local thresholding methods such as adaptive and Sauvola thresholding methods, may jeopardize the performance for our samples in Fig. 8-d. In addition, thresholding methods tend to capture the edge and neglect the inner part of the objects.

Despite the significant progress, there remain many challenges for future work. Firstly, though SEM shows more details, it takes a longer time for sample preparation and microscopic photography than an optical camera. More comprehensive datasets of microplastics might be established in the future with the help of advanced SEM automation techniques. Larger datasets also make it possible to identify and extract microplastics from a complicated background in environmental samples. Secondly, our models were trained on a small dataset and they have a better performance on a single dataset than the mixed datasets. It might be a good way to use self-supervised learning and other up-to-date models (Attention U-Net, TransUNet (Chen et al., n.d.)) to reduce the overfitting and achieve better overall performance. For example, TransUNet, combined with the Transformer architecture, can alleviate the influence of limitation of convolution operations: the intrinsic locality (Chen et al., n.d.). Thirdly, the metrics we used are not robust to slight misalignment (Wegmayr et al., 2020). For example, Fig. 8-c with a 3 × 3 Gaussian blur has less false positive, but the score is lower than Fig. 8-a, b since a smaller kernel gives a thinner edge. In addition, although Fig. 6-c has higher scores than Fig. 8, it misses the top two beads in juxtaposition. Finally, each micrograph contains only one type of microplastics in the datasets and the shape classification network is independent of image segmentation at the present stage. Micrographs with microplastics in multiple shapes and chemical compositions in future work would enable quantification and classification via a single end-to-end multi-class instance segmentation neural network.

In conclusion, our experiments produced hundreds of SEM images of microplastics in different shapes and chemical compositions from daily supplies. Manual annotation is given for each image to constitute the first open-source SEM datasets for microplastics segmentation. Deep learning methods have been used for microplastics segmentation and shape classification. The promising result tremendously facilitates automatic quantification and classification of microplastics, therefore helps monitor microplastic pollution more accurately and effectively.

CRediT authorship contribution statement

Bin Shi: Conceptualization, Methodology, Software, Data Curation, Writing. **Medhavi Patel**: Methodology, Investigation, Resources, Writing. **Dian Yu**, **Jihui Yan**: Methodology, Investigation, Resources. **Zhengyu Li**: Methodology, Data Curation. **David Petriw**, **Thomas Pruyn**: Data Curation. **Kelsey Smyth**: Resources, Review and Editing. **Elodie Passeport**, **R.J.Dwayne Miller**: Supervision, Review and Editing. **Jane Y. Howe**: Conceptualization, Methodology, Resources, Supervision, Review and Editing.

Declaration of competing interest

The authors declare that they have no known competing financial interests or personal relationships that could have appeared to influence the work reported in this paper.

Acknowledgements

The project is supported by the WaterSeed Fund from Institute for Water Innovation, University of Toronto and by the Natural Sciences and Engineering Research Council of Canada (NSERC)'s Discovery Grant. Electron microscopy was performed at the Open Centre for the Characterization of Advanced Materials (OCCAM), funded by the Canada Foundation for Innovation. Experiments were performed in part with the help of Dr. Jason Tam. This research was enabled in part by support provided by Compute Canada.

References

Anger, P.M., Prechtl, L., Elsner, M., Niessner, R., Ivleva, N.P., 2019. Implementation of an open source algorithm for particle recognition and morphological characterisation for microplastic analysis by means of Raman microspectroscopy. Anal. Methods 11 (27), 3483–3489. https://doi.org/10.1039/C9AY01245A.

Aversa, R., Modarres, M.H., Cozzini, S., Ciancio, R., Chiusole, A., 2018. The first annotated set of scanning electron microscopy images for nanoscience. Sci. Data 5 (1), 1–10. https://doi.org/10.1038/sdata.2018.172.

Badrinarayanan, V., Kendall, A., Cipolla, R., 2017. Segnet: a deep convolutional encoder-decoder architecture for image segmentation. IEEE Trans. Pattern Anal. Mach. Intell. 39 (12), 2481–2495. https://doi.org/10.1109/TPAMI.2016.2644615.

Browne, M.A., Crump, P., Niven, S.J., Teuten, E., Tonkin, A., Galloway, T., Thompson, R., 2011. Accumulation of microplastic on shorelines woldwide: sources and sinks. Environ. Sci. Technol. 45 (21), 9175–9179. https://doi.org/10.1021/es201811s.

Burnstock, A., Jones, C., 2000. Scanning electron microscopy techniques for imaging materials from paintings. Radiation in Art and Archeometry, pp. 202–231 https://doi.org/10.1016/B978-044450487-6/50056-0.

Chen, L.-C., Papandreou, G., Kokkinos, I., Murphy, K., Yuille, A.L., 2017. DeepLab: semantic image segmentation with deep convolutional nets, atrous convolution, and fully connected CRFs. IEEE Trans. Pattern Anal. Mach. Intell. 40 (4), 834–848. https://doi.org/10.1109/TPAMI.2017.2699184.

Chen, L., Strauch, M., Merhof, D., 2019. Instance segmentation of biomedical images with an object-aware embedding learned with local constraints. International Conference on Medical Image Computing and Computer-Assisted Intervention. Springer, pp. 451–459 https://doi.org/10.1007/978-3-030-32239-7_50.

Chen, J., Lu, Y., Yu, Q., Luo, X., Adeli, E., Wang, Y., Lu, L., Yuille, A.L., Zhou, Y., .. TransUNet: transformers make strong encoders for medical image segmentation. arXiv preprint arXiv: 2102.04306. URL https://arxiv.org/abs/2102.04306.

Cole, M., Webb, H., Lindeque, P.K., Fileman, E.S., Halsband, C., Galloway, T.S., 2014. Isolation of microplastics in biota-rich seawater samples and marine organisms. Sci. Rep. 4 (1), 1–8. https://doi.org/10.1038/srep04528.

Dalal, N., Triggs, B., 2005. Histograms of oriented gradients for human detection. 2005 IEEE computer society conference on computer vision and pattern recognition (CVPR'05). vol. 1. IEEE, pp. 886–893. https://doi.org/10.1109/CVPR.2005.177.

De, S., Bhattacharyya, S., Chakraborty, S., Dutta, P., 2016. Hybrid Soft Computing for Multilevel Image and Data Segmentation. Springer International Publishing, pp. 29–33 https://doi.org/10.1007/978-3-319-47524-0 Ch. 2.2.

Desforges, J.-P.W., Galbraith, M., Dangerfield, N., Ross, P.S., 2014. Widespread distribution of microplastics in subsurface seawater in the NE Pacific Ocean. Mar. Pollut. Bull. 79 (1–2), 94–99. https://doi.org/10.1016/j.marpolbul.2013.12.035.

Digka, N., Tsangaris, C., Kaberi, H., Adamopoulou, A., Zeri, C., 2018. Microplastic abundance and polymer types in a mediterranean environment. Proceedings of the international conference on microplastic pollution in the Mediterranean Sea. Springer, pp. 17–24 https://doi.org/10.1007/978-3-319-71279-6_3.

do Sul, J.A.I., Costa, M.F., 2014. The present and future of microplastic pollution in the marine environment. Environ. Pollut. 185, 352–364. https://doi.org/10.1016/j.envpol.2013.10.036.

Eerkes-Medrano, D., Thompson, R.C., Aldridge, D.C., 2015. Microplastics in freshwater systems: a review of the emerging threats, identification of knowledge gaps and prioritisation of research needs. Water Res. 75, 63–82. https://doi.org/10.1016/j.watres.2015.02.012.

Free, C.M., Jensen, O.P., Mason, S.A., Eriksen, M., Williamson, N.J., Boldgiv, B., 2014. High-levels of microplastic pollution in a large, remote, mountain lake. Mar. Pollut. Bull. 85 (1), 156–163. https://doi.org/10.1016/j.marpolbul.2014.06.001.

Goldstein, J.I., Newbury, D.E., Michael, J.R., Ritchie, N.W., Scott, J.H.J., Joy, D.C., 2018. Scanning Electron Microscopy and X-ray Microanalysis. Springer, New York https://doi.org/10.1007/978-1-4939-6676-9 Ch. 9.1,12, pp. 134–139,173–185.

Haberl, M.G., Churas, C., Tindall, L., Boassa, D., Phan, S., Bushong, E.A., Madany, M., Akay, R., Deerinck, T.J., Peltier, S.T., et al., 2018. CDeep3M—Plug-and-Play cloud-based deep learning for image segmentation. Nat. Methods 15 (9), 677–680. https://doi.org/10.1038/s41592-018-0106-z.

He, K., Zhang, X., Ren, S., Sun, J., 2016. Deep residual learning for image recognition. Proceedings of the IEEE Conference on Computer Vision and Pattern Recognition, pp. 770–778 https://doi.org/10.1109/CVPR.2016.90.

He, K., Gkioxari, G., Dollár, P., Girshick, R., 2017. Mask R-CNN. Proceedings of the IEEE international conference on computer vision, pp. 2961–2969 https://doi.org/10.1109/ICCV.2017.322.

Hidalgo-Ruz, V., Gutow, L., Thompson, R.C., Thiel, M., 2012. Microplastics in the marine environment: a review of the methods used for identification and quantification. Environmental science & technology 46 (6), 3060–3075. https://doi.org/10.1021/es2031505.

Ibtehaz, N., Rahman, M.S., 2020. MultiResUNet: rethinking the U-Net architecture for multimodal biomedical image segmentation. Neural Netw. 121, 74–87. https://doi.org/10.1016/j.neunet.2019.08.025.

Isobe, A., Kubo, K., Tamura, Y., Nakashima, E., Fujii, N., et al., 2014. Selective transport of microplastics and mesoplastics by drifting in coastal waters. Mar. Pollut. Bull. 89 (1–2), 324–330. https://doi.org/10.1016/j.marpolbul.2014.09.041.

Isobe, A., Uchiyama-Matsumoto, K., Uchida, K., Tokai, T., 2017. Microplastics in the Southern Ocean. Mar. Pollut. Bull. 114 (1), 623–626. https://doi.org/10.1016/j.marpolbul.2016.09.037.

Joy, D.C., Joy, C.S., 1996. Low voltage scanning electron microscopy. Micron 27 (3–4), 247–263. https://doi.org/10.1016/0968-4328(96)00023-6.

Khadangi, A., Boudier, T., Rajagopal, V., 2021. EM-net: Deep learning for electron microscopy image segmentation. 2020 25th International Conference on Pattern Recognition (ICPR). IEEE, pp. 31–38 https://doi.org/10.1109/ICPR48806.2021.9413098.

Kong, S., Fowlkes, C.C., 2018. Recurrent pixel embedding for instance grouping. Proceedings of the IEEE Conference on Computer Vision and Pattern Recognition, pp. 9018–9028 https://doi.org/10.1109/CVPR.2018.00940.

Lin, T.-Y., Dollár, P., Girshick, R., He, K., Hariharan, B., Belongie, S., 2017. Feature pyramid networks for object detection. Proceedings of the IEEE conference on computer vision and pattern recognition, pp. 2117–2125 https://doi.org/10.1109/CVPR.2017.106.

Long, J., Shelhamer, E., Darrell, T., 2015. Fully convolutional networks for semantic segmentation. Proceedings of the IEEE Conference on Computer Vision and Pattern Recognition, pp. 3431–3440 https://doi.org/10.1109/TPAMI.2016.2572683.

Lorenzo-Navarro, J., Castrillón-Santana, M., Gómez, M., Herrera, A., Marn-Reyes, P.A., 2018. Automatic counting and classification of microplastic particles. ICPRAM 2018-Proceedings of the 7th International Conference on Pattern Recognition Applications and Methods https://doi.org/10.5220/0006725006460652.

Lorenzo-Navarro, J., Castrillón-Santana, M., Santesarti, E., De Marsico, M., Martnez, I., Raymond, E., Gómez, M., Herrera, A., 2020. SMACC: a system for microplastics automatic counting and classification. IEEE Access 8, 25249–25261. https://doi.org/10.1109/ACCESS.2020.2970498.

Lorenzo-Navarro, J., Castrillón-Santana, M., Sánchez-Nielsen, E., Zarco, B., Herrera, A., Martnez, I., Gómez, M., 2021. Deep learning approach for automatic microplastics counting and classification. Sci. Total Environ. 765, 142728. https://doi.org/10.1016/j.scitotenv.2020.142728.

Lusher, A.L., Burke, A., O'Connor, I., Officer, R., 2014. Microplastic pollution in the Northeast Atlantic Ocean: validated and opportunistic sampling. Mar. Pollut. Bull. 88 (1–2), 325–333. https://doi.org/10.1016/j.marpolbul.2014.08.023.

Lusher, A.L., Tirelli, V., O'Connor, I., Officer, R., 2015. Microplastics in Arctic polar waters: the first reported values of particles in surface and sub-surface samples. Sci. Rep. 5, 14947. https://doi.org/10.1038/srep14947.

Matuszewski, D.J., Sintorn, I.-M., 2019. Reducing the U-Net size for practical scenarios: virus recognition in electron microscopy images. Comput. Methods Prog. Biomed. 178, 31–39. https://doi.org/10.1016/j.cmpb.2019.05.026.

Minaee, S., Boykov, Y.Y., Porikli, F., Plaza, A.J., Kehtarnavaz, N., Terzopoulos, D., 2021. Image segmentation using deep learning: a survey. IEEE Trans. Pattern Anal. Mach. Intell. https://doi.org/10.1109/TPAMI.2021.3059968.

Naji, A., Nuri, M., Vethaak, A.D., 2018. Microplastics contamination in molluscs from the northern part of the Persian Gulf. Environ. Pollut. 235, 113–120. https://doi.org/10.1016/j.envpol.2017.12.046.

Nuelle, M.-T., Dekiff, J.H., Remy, D., Fries, E., 2014. A new analytical approach for monitoring microplastics in marine sediments. Environ. Pollut. 184, 161–169. https://doi.org/10.1016/j.envpol.2013.07.027.

Otsu, N., 1979. A threshold selection method from gray-level histograms. IEEE Trans. Syst. Man Cybern. 9 (1), 62–66. https://doi.org/10.1109/TSMC.1979.4310076.

Prata, J.C., Reis, V., Matos, J.T., da Costa, J.P., Duarte, A.C., Rocha-Santos, T., 2019. A new approach for routine quantification of microplastics using Nile Red and automated software (MP-VAT). Sci. Total Environ. 690, 1277–1283. https://doi.org/10.1016/j.scitotenv.2019.07.060.

Primpke, S., Lorenz, C., Rascher-Friesenhausen, R., Gerdts, G., 2017. An automated approach for microplastics analysis using focal plane array (FPA) FTIR microscopy and image analysis. Anal. Methods 9 (9), 1499–1511. https://doi.org/10.1039/C6AY02476A.

Rahman, A., Sarkar, A., Yadav, O.P., Achari, G., Slobodnik, J., 2020. Potential human health risks due to environmental exposure to microplastics and knowledge gaps: a scoping review. Sci. Total Environ. 143872. https://doi.org/10.1016/j.scitotenv.2020.143872.

Ronneberger, O., Fischer, P., Brox, T., 2015. U-Net: convolutional networks for biomedical image segmentation. International Conference on Medical image computing and computer-assisted intervention. Springer, pp. 234–241 https://doi.org/10.1007/978-3-319-24574-4_28.

Rudnaya, M., Mattheij, R., Maubach, J., 2010. Evaluating sharpness functions for automated scanning electron microscopy. J. Microsc. 240 (1), 38–49. https://doi.org/10.1111/j.1365-2818.2010.03383.x.

Sait, S.T., Sørensen, L., Kubowicz, S., Vike-Jonas, K., Gonzalez, S.V., Asimakopoulos, A.G., Booth, A.M., 2021. Microplastic fibres from synthetic textiles: environmental degradation and additive chemical content. Environ. Pollut. 268, 115745. https://doi.org/10.1016/j.envpol.2020.115745.

Sauvola, J., Pietikäinen, M., 2000. Adaptive document image binarization. Pattern Recogn. 33 (2), 225–236. https://doi.org/10.1016/S0031-3203(99)00055-2.

Schorb, M., Haberbosch, I., Hagen, W.J., Schwab, Y., Mastronarde, D.N., 2019. Software tools for automated transmission electron microscopy. Nat. Methods 16 (6), 471–477. https://doi.org/10.1038/s41592-019-0396-9.

Shim, W.J., Hong, S.H., Eo, S.E., 2017. Identification methods in microplastic analysis: a review. Anal. Methods 9 (9), 1384–1391. https://doi.org/10.1039/C6AY02558G.

Siddique, N., Paheding, S., Elkin, C.P., Devabhaktuni, V., 2021. U-Net and its variants for medical image segmentation: a review of theory and applications. IEEE Access https://doi.org/10.1109/ACCESS.2021.3086020.

Simon, M., van Alst, N., Vollertsen, J., 2018. Quantification of microplastic mass and removal rates at wastewater treatment plants applying Focal Plane Array (FPA)-based Fourier Transform Infrared (FT-IR) imaging. Water Res. 142, 1–9. https://doi.org/10.1016/j.watres.2018.05.019.

Simonyan, K., Zisserman, A., .. Very deep convolutional networks for large-scale image recognition, 3rd International Conference on Learning Representations, ICLR. Conference Track Proceedings. URL https://arxiv.org/abs/1409.1556.

Smyth, K., Drake, J., Li, Y., Rochman, C., Van Seters, T., Passeport, E., 2021. Bioretention cells remove microplastics from urban stormwater. Water Res. 191, 116785. https://doi.org/10.1016/j.watres.2020.116785.

Song, Y.K., Hong, S.H., Jang, M., Han, G.M., Rani, M., Lee, J., Shim, W.J., 2015. A comparison of microscopic and spectroscopic identification methods for analysis of microplastics in environmental samples. Mar. Pollut. Bull. 93 (1–2), 202–209. https://doi.org/10.1016/j.marpolbul.2015.01.015.

Strungaru, S.-A., Jijie, R., Nicoara, M., Plavan, G., Faggio, C., 2019. Micro-(nano) plastics in freshwater ecosystems: abundance, toxicological impact and quantification methodology. TrAC Trends Anal. Chem. 110, 116–128. https://doi.org/10.1016/j.trac.2018.10.025.

Van Cauwenberghe, L., Vanreusel, A., Mees, J., Janssen, C.R., 2013. Microplastic pollution in deep-sea sediments. Environ. Pollut. 182, 495–499. https://doi.org/10.1016/j.envpol.2013.08.013.

von der Esch, E., Kohles, A.J., Anger, P.M., Hoppe, R., Niessner, R., Elsner, M., Ivleva, N.P., 2020. TUM-ParticleTyper: a detection and quantification tool for automated analysis of (microplastic) particles and fibers. Plos one 15 (6), e0234766. https://doi.org/10.1371/journal.pone.0234766.

Wagner, M., Scherer, C., Alvarez-Muñoz, D., Brennholt, N., Bourrain, X., Buchinger, S., Fries, E., Grosbois, C., Klasmeier, J., Marti, T., et al., 2014. Microplastics in freshwater ecosystems: what we know and what we need to know. Environ. Sci. Eur. 26 (1), 12. https://doi.org/10.1186/s12302-014-0012-7.

Wang, Z.-M., Wagner, J., Ghosal, S., Bedi, G., Wall, S., 2017. SEM/EDS and optical microscopy analyses of microplastics in ocean trawl and fish guts. Sci. Total Environ. 603, 616–626. https://doi.org/10.1016/j.scitotenv.2017.06.047.

Wang, W., Ge, J., Yu, X., 2020. Bioavailability and toxicity of microplastics to fish species: a review. Ecotoxicol. Environ. Saf. 189, 109913. https://doi.org/10.1016/j.ecoenv.2019.109913.

Wegmayr, V., Sahin, A., Saemundsson, B., Buhmann, J., 2020. Instance segmentation for the quantification of microplastic fiber images. Proceedings of the IEEE/CVF Winter Conference on Applications of Computer Vision, pp. 2210–2217 https://doi.org/10.1109/WACV45572.2020.9093352.

Werbowski, L.M., Gilbreath, A.N., Munno, K., Zhu, X., Grbic, J., Wu, T., Sutton, R., Sedlak, M.D., Deshpande, A.D., Rochman, C.M., 2021. Urban stormwater runoff: a major pathway for anthropogenic particles, black rubbery fragments, and other types of microplastics to urban receiving waters. ACS ES&T Water 1 (6), 1420–1428. https://doi.org/10.1021/acsestwater.1c00017.

Woodall, L.C., Sanchez-Vidal, A., Canals, M., Paterson, G.L., Coppock, R., Sleight, V., Calafat, A., Rogers, A.D., Narayanaswamy, B.E., Thompson, R.C., 2014. The deep sea is a major sink for microplastic debris. R. Soc. Open Sci. 1 (4), 140317. https://doi.org/10.1098/rsos.140317.

Xing, F., Xie, Y., Su, H., Liu, F., Yang, L., 2017. Deep learning in microscopy image analysis: a survey. IEEE Trans. Neural Netw. Learn. Syst. 29 (10), 4550–4568. https://doi.org/10.1109/TNNLS.2017.2766168.

Yildirim, B., Cole, J.M., 2021. Bayesian particle instance segmentation for electron microscopy image quantification. J. Chem. Inf. Model. 61 (3), 1136–1149. https://doi.org/10.1021/acs.jcim.0c01455.

Zhu, Y., Yeung, C.H., Lam, E.Y., 2020. Holographic classifier: deep learning in digital holography for automatic micro-objects classification. 2020 IEEE 18th International Conference on Industrial Informatics (INDIN). vol. 1. IEEE, pp. 515–520. https://doi.org/10.1109/INDIN45582.2020.9442146.